Crystal Structures of Spin Labeled T4 Lysozyme Mutants: Implications for the Interpretation of EPR Spectra in Terms of Structure†

Ralf Langen,‡,§,|| Kyoung Joon Oh,‡,⊥,|| Duilio Cascio,*,# and Wayne L. Hubbell*,‡

Jules Stein Eye Institute and Department of Chemistry and Biochemistry, University of California, Los Angeles, California 90095-7008, and UCLA-DOE Laboratory of Structural Biology and Molecular Medicine, 201 Boyer, Box 951570, Los Angeles, California 90095-1570

Received March 16, 2000; Revised Manuscript Received May 13, 2000

ABSTRACT: High resolution (1.43−1.8 Å) crystal structures and the corresponding electron paramagnetic resonance (EPR) spectra were determined for T4 lysozyme derivatives with a disulfide-linked nitroxide side chain [-CH_2-S-S-CH_2-(3-[2,2,5,5-tetramethyl pyrroline-1-oxyl]) ≡ R1] substituted at solvent-exposed helix surface sites (Lys65, Arg80, Arg119) or a tertiary contact site (Val75). In each case, electron density is clearly resolved for the disulfide group, revealing distinct rotamers of the side chain, defined by the dihedral angles X_1 and X_2. The electron density associated with the nitroxide ring in the different mutants is inversely correlated with its mobility determined from the EPR spectrum. Residue 80R1 assumes a single g^+g^+ conformation ($X_1 = 286$, $X_2 = 294$). Residue 119R1 has two EPR spectral components, apparently corresponding to two rotamers, one similar to that for 80R1 and the other in a tg^- conformation ($X_1 = 175$, $X_2 = 54$). The latter state is apparently stabilized by interaction of the disulfide with a Gln at i + 4, a situation also observed at 65R1. R1 residues at helix surface site 65 and tertiary contact site 75 make intra- as well as intermolecular contacts in the crystal and serve to identify the kind of molecular interactions possible for the R1 side chain. A single conformation of the entire 75R1 side chain is stabilized by a variety of interactions with the nitroxide ring, including hydrophobic contacts and two unconventional C−H···O hydrogen bonds, one in which the nitroxide acts as a donor (with tyrosine) and the other in which it acts as an acceptor (with phenylalanine). The interactions revealed in these structures provide an important link between the dynamics of the R1 side chain, reflected in the EPR spectrum, and local protein structure. A library of such interactions will provide a basis for the quantitative interpretation of EPR spectra in terms of protein structure and dynamics.

Site-directed spin labeling (SDSL)[1] has become a powerful tool for probing structure and conformational dynamics of both water-soluble and membrane proteins of arbitrary molecular weight (for reviews, see refs *1*−*4*). The basic strategy of SDSL involves the substitution of a cysteine for the native residue, followed by modification of the reactive SH group with a selective nitroxide reagent. The most commonly employed reagent is a methanethiosulfonate derivative that generates the disulfide-linked nitroxide side chain, designated R1 (Figure 1), although other reagents have been employed (*5*).

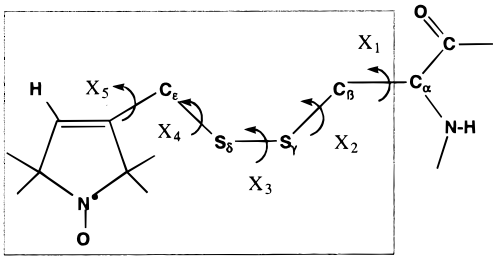

Side Chain R1

FIGURE 1: Structure of the R1 side chain, indicating the dihedral angles X_1−X_5 and the 4-H atom on the nitroxide ring.

Analysis of the electron paramagnetic resonance (EPR) spectrum of R1 in a protein provides direct experimental measures for side chain solvent accessibility, polarity of the local environment, and side chain mobility. Solvent accessibility is quantitatively determined from the collision frequency of the nitroxide side chain with paramagnetic

† This work was supported by NIH Grant EY05216 (W.L.H.), Jules Stein Professorship Endowment (W.L.H.), the Bruce Ford Bundy and Anne Smith Bundy Foundation (W.L.H.), National Research Service Award EY06809 (to R.L.), and the DOE Laboratory of Structural Biology (D.C.).

* To whom correspondence should be addressed: Jules Stein Eye Institute, UCLA School of Medicine, Los Angeles, CA 90095-7008. Telephone: 310/206-8830. Fax: 310/794-2144. E-mail: hubbellw@jsei.ucla.edu.

‡ Jules Stein Eye Institute, UCLA School of Medicine.

|| These authors contributed equally to this work.

§ Current address: Department of Biochemistry and Molecular Biology, University of Southern California, Los Angeles, CA 90033.

⊥ Current Address: Dana-Farber Cancer Institute, 44 Binney St., Boston, MA 02115.

UCLA-DOE Laboratory of Structural Biology and Molecular Medicine, 201 Boyer, Box 951570, Los Angeles, CA 90095-1570. Telephone: 310/825-1551. Fax: 310/206-3914. E-mail: cascio@uclaue.mbi.ucla.edu.

[1] Abbreviations: DTT, dithiothreitol; EDTA, ethylenediaminetetraacetic acid; EPR, electron paramagnetic resonance; LB, Luria Broth; SDSL, site-directed spin labeling; T4L, T4 lysozyme.

10.1021/bi000604f CCC: $19.00
Published on Web 06/27/2000

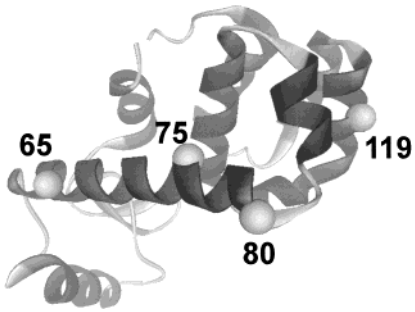

FIGURE 2: Ribbon diagram of T4L. Sites where R1 was substituted are identified as spheres on the α-carbons.

reagents in solution (*6*), and environment polarity is deduced from features of the EPR spectrum at low temperature (*7*). The sequence dependence of accessibility and polarity has proven to be a robust indicator of local secondary structure and its topography in a protein fold, and many applications have been published for both helical and β-sheet structures (*1*−*3*, *8*).

The identification of R1 dynamic modes in a protein structure from the EPR spectrum is still in its infancy. At present, EPR spectra are described in terms of the qualitative descriptor "mobility" that is intended to include effects of both amplitude and rate. Simple measures of mobility include the inverse central line width and the spectral second moment (*2*, *9*). In T4L, residue mobility alone can generally distinguish helix surface sites, tertiary contact sites, loop sites, and buried sites. Helix surface sites can be subdivided based on mobility into C-terminal, N-terminal, and interior sites (those not at the end of the helix) (*9*). Like accessibility, the periodic dependence of mobility along a sequence can be used to identify secondary structure and protein topography (*9*).

Although this qualitative level of interpretation provides important structural information, the spectral line shapes of R1 side chains apparently encode finer details of the local structure and perhaps dynamics. For example, the spectra of R1 at different solvent-exposed interior sites on T4L helices are unique, even though the nearest neighbor residues may be identical. Moreover, the spectra at many of the sites are multicomponent, reflecting multiple motional states of the side chain (*9*). The structural origins of the distinct "fingerprint" spectra at each site are unknown but clearly must be understood to make further progress in interpretation of the EPR spectra in terms of structure.

To understand the relationship between side chain mobility and the details of protein structure and dynamics, it is essential to determine the preferred conformations of the R1 side chain itself and to elucidate its interactions with the main chain and side chain atoms. Such information will provide a basis for constraining spectral simulations aimed at deconvoluting the dynamic modes of the R1 side chain (*10*, *11*) and guide the development of new nitroxide side chains designed to report specific dynamic or structural features.

To this end, the present study reports high-resolution structures of T4L derivatives bearing the R1 side chain at either 65 and 80, 119, or 75 (Figure 2). These sites, all located in helical sequences, were chosen as representatives of helix interior sites, C-terminal sites, multicomponent helix interior sites and tertiary contact sites, respectively. As reported previously, these classes have distinctive mobility characteristics that permit their identification on this basis alone (*5*, *9*).

For each R1 side chain, electron density is clearly resolved for the disulfide group, and preferred conformations about X_1 and X_2 can be identified. The ordered state for the disulfide is apparently due to interactions with main chain atoms and, in some cases, with a Gln residue at the i + 4 position. In general, a high mobility for the nitroxide, as judged by the EPR spectrum, is correlated with little or no resolved electron density for the nitroxide ring itself.

For 119R1, two conformations of the side chain are seen that account for the two spectral populations. Residues 65 and 75 are located at crystal contact sites. Nevertheless, they serve to identify the nature of molecular interactions possible for the R1 side chain. In 75R1, the nitroxide ring acts as both a donor and acceptor in forming two CH···O hydrogen bonds between tyrosine and phenylalanine. These nonclassical hydrogen bonds may be the principal interactions leading to immobilization at this solvent-exposed tertiary contact site.

EXPERIMENTAL PROCEDURES

Construction of T4 Lysozyme Mutants. The cysteine-less pseudo-wild-type T4L gene containing the substitutions C54T and C97A (*12*) was kindly provided by F. W. Dahlquist (University of Oregon). Mutant T4Ls with substitutions K65C, R80C, R119C, and V75C were prepared as described earlier (*5*, *9*). The double mutant K65C/R80C was prepared by sequential introduction of the Cys residues at positions 65 and 80 by the overlap extension method (*13*). The nucleotide sequence was verified by sequencing the entire gene.

Expression, Purification, and Spin Labeling of T4 Lysozyme Mutants. All mutants of T4L were expressed in *Escherichia coli* K38 cells as previously described (*14*) with some modifications. Briefly, K38 cells containing mutant plasmids were cultured overnight in LB medium containing 100 μg/mL ampicillin. LB medium (500 mL) containing 100 μg/mL ampicillin was inoculated with 15 mL of the overnight culture. The cells were grown at 37 °C until the optical density at 580 nm reached ∼1.0−1.2. Protein expression was induced by adding isopropyl β-thiogalactoside (1 mM). After 1 h, the cells were harvested by centrifugation, and the cell pellets were frozen at −20 °C for storage. For protein purification, cell pellets were thawed and resuspended in a buffer containing 20 mM Tris, 1 mM EDTA, 0.02% (w/v) NaN_3, and 10 mM DTT, pH 7.6. The bacterial cell walls were disrupted by sonication on ice, and the cell debris was removed by centrifugation. The supernatant was then loaded on a Pharmacia Resource S column equilibrated with the buffer containing 0.5 mM DTT. The protein was eluted with a gradient of 0−1 M NaCl. The T4L fraction was collected, DTT was added to a final concentration of 5−10 mM, and the sample was frozen for storage at −80 °C.

For spin labeling, DTT was removed by gel filtration on a PD-10 column (Pharmacia), eluting with a buffer containing 20 mM Tris, 150 mM NaCl, 1 mM EDTA, and 0.02% (w/v) NaN_3, pH 7.6. The T4L mutants were immediately reacted with an approximately 10-fold excess of [3-methyl-(2,2,5,5, tetramethyl-pyrrolidinyl-1-oxyl] methanethiosulfonate (a gift of Kálmán Hideg) at room temperature. The

Table 1: X-ray Data Collection and Refinement Statistics

	V75R1	R119R1	K65R1/R80R1
R_{cryst}	0.17	0.19	0.18
R_{free}	0.22	0.23	0.22
completeness	99.7	99.5	98.4
res limit (Å)	1.5 (BNL-X12B)	1.43 (BNL-X8C)	1.8 (UCLA-RAXISIV)
wavelength (Å)	1.2546	0.9780	1.5418
temp (K)	100	100	298
no. of water mol	81	240	51
reflect obs	445 260	436 152	140 664
uniq reflect	33 102	37 322	19 743
R_{sym} (%)	7.9	6.3	6.2
RMSD bonds length (Å)	0.008	0.009	0.007
RMSD bonds angle (deg)	1.2	1.2	1.2
space group	$P3_221$	$P3_221$	$P3_221$
cell dimen (Å)[a]			
a	60.30	60.01	60.02
b	60.30	60.01	60.02
c	95.53	95.44	96.94

[a] The space group of pseudo-WT T4 lysozyme is $P3_221$, and the cell dimensions are $a = 61.2$, $b = 61.2$, $c = 96.8$ (*15*).

reaction was allowed to continue overnight, and excess reagent was then removed by gel filtration on a PD-10 column in the same buffer used for spin labeling.

Crystallization of Spin Labeled T4L Cysteine Mutants. Crystals of spin labeled T4L mutants were grown at 4 °C by the hanging drop method using 2 M phosphate as a precipitant according to conditions described previously (*15*), with some modifications. Briefly, reservoir buffers ranging from pH 6.2 to 7.2 were prepared by mixing 2 M solutions of NaH_2PO_4 and 2M K_2HPO_4, each containing 150 mM NaCl and 0.04% (w/v) NaN_3 and saturated with bis-2-ethyl disulfide. Protein hanging drops were set up at 4 °C over a 2-mL reservoir buffer by mixing 10 μL of reservoir buffer at various pH values with an equal volume of spin labeled T4L solution (concentration 10−30 mg/mL). Crystals appeared within a few weeks. Diffraction-quality crystals were larger than 400 μm in the longest dimension.

Diffraction and Refinement. Crystals of mutants 119R1 and 75R1 were cryoprotected (B. Mooers and B. Matthews, personal communication) and flash-frozen in a nitrogen gas stream at 100K (X-TREAM from Molecular Structure Corp., The Woodlands, Texas). The crystals were transported in a cryo-shipper to Brookhaven National Laboratory. Data were collected at 100 K (Oxford Cryosystems) at beamlines X12B and X8C (National Synchrotron Light Source, Brookhaven National Laboratory), processed with DENZO and reduced with SCALEPACK (*16*). Crystals of the double mutant 65R1/80R1 were mounted in a glass capillary, and data were collected at 298 K on a RAXIS-IV image plate detector (RIGAKU) using Cu-Kα X-rays from a rotating anode (RIGAKU) operated at 5kW and focused with Yale mirrors (from Molecular Structure Corp., The Woodlands, Texas).

The three mutant proteins crystallized in the same space group and with similar cell dimensions as the T4 lysozyme "pseudo-wild type" (*15*). Therefore, the structures were refined with X-PLOR (*17*) using Protein Data Bank ID code 3LZM as the starting model. The model was truncated to glycine at the site of each mutation. Rigid body refinement, followed by positional and B factor refinement of the initial model was performed using X-PLOR, first against data to 2.0 A. The refinement was monitored using the free R factor. A randomly selected subset (5%) of the data was saved before the start of the refinement for the free R factor calculation. Further cycles of rebuilding and refinement were carried out at the highest resolution of each data set using SHELXL (*18*). After the R factor dropped below 22%, the R1 side chain was manually added and modeled using the $2F_o-F_c$ and F_o-F_c electron density maps with the program O (*19*). Table 1 lists the data collection and refinement statistics.

EPR Spectroscopy. EPR spectra were recorded on a Varian E-109 spectrometer fitted with a two-loop one gap resonator (*20*). All spectra were obtained at 2 mW incident microwave power using a field modulation of ~1 G. Solution spectra were obtained in 30% sucrose (*9*). To obtain isotropic powder EPR spectra, several crystals were crushed in the mother liquor. In each case, the spectra were found to be independent of the orientation of the sample in the resonator. Although the double mutant 65R1/80R1 was used for crystallography, the EPR spectra for R1 at the individual sites were obtained from the single mutants K65R1 and R80R1. The EPR spectrum of crystals for the 65R1/80R1 double mutant is in good agreement with the sum of the respective spectra for the single mutants 65R1 and 80R1, indicating that the structures of the spin labels in the single mutant crystals are similar to those in the double mutant.

RESULTS

The EPR spectra of the spin labeled mutants in 30% sucrose solution (thin trace) and in a polycrystalline suspension (thick trace) are compared in Figure 3. The spectra in 30% sucrose were previously published (*5*, *9*) and are reproduced here for comparative purposes. In 30% sucrose, the effect of protein rotational motion on the EPR spectra is minimized, and the spectra reflect primarily motion of the nitroxide relative to the protein (*9*). Thus, comparison of the solution and crystal spectra indicates the effect of the lattice environment on the side chain motion.

The X-ray diffraction data collection and refinement characteristics for all mutants are summarized in Table 1. The double mutant 65R1/80R1 was used for diffraction rather than the corresponding single mutants, because the crystals from the latter were too small, although they had the same space group and shape as those from the double mutant. Because crystals of 119R1 and 75R1 exhibited decay at room

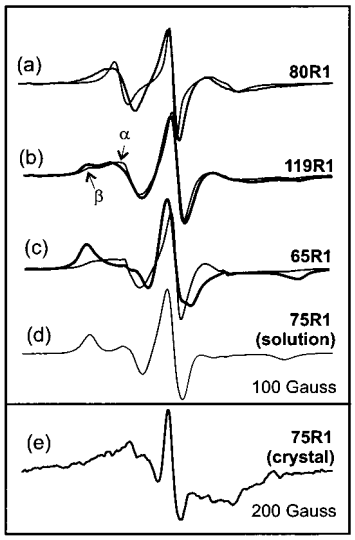

FIGURE 3: EPR spectra of the indicated spin labeled T4 lysozymes (panels a−e). In each panel, spectra obtained in 30% sucrose solution (thin line) and in a polycrystalline suspension (thick line) are superimposed for comparison. Scan width is 100 G in (panels a−c), and 200 G in (panel e). Spectra are normalized to the same amplitude for ease of comparison.

temperature, data were also collected at low temperature (100 K) using synchrotron radiation. These conditions enhanced the overall resolution but did not cause significant structural differences in terms of protein or spin label structure. Only the high-resolution structures from the 100 K data are presented below (1.43 Å for 119R1 and 1.5 Å for 75R1). For each mutant, the final structure was essentially superimposable with that of wild-type T4L except at the substitution site (see RMS deviations in Table 1).

Structure of 80R1. The EPR spectrum of 80R1 in solution (Figure 3a, thin trace) reflects a high mobility of the nitroxide, typical of solvent-exposed R1 residues near the C-terminal end of helices. In the crystal (Figure 3a, heavy trace), the spectrum is broader but of similar general shape. The broadening probably has a contribution from a damped backbone motion in the crystal but also from a magnetic dipolar interaction with a second R1 in a symmetry-related molecule (distance 15−20 Å). Under any circumstance, the spectrum in the crystalline state, like that in solution, reflects a relatively high mobility of the nitroxide ring, supporting the conclusion that the conformation of the side chain is similar in both states and that no salient new interactions are established in the crystal lattice.

An electron density map and a corresponding space-filling model for the R1 side chain in 80R1 are shown in Figure 4a and b, respectively. A conspicuous feature of the electron density map is the absence of density corresponding to the nitroxide ring at the 1.3 σ contour level. This is in accord with the high mobility of the R1 nitroxide at this site, as inferred from the EPR spectrum, because the thermal motion averages the electron density of the ring over a larger volume. However, electron density is evident for both sulfur atoms of the disulfide group. The observed orientation of the disulfide corresponds to a conformation with $X_1 \approx 286°$, $X_2 \approx 294°$, a relaxed g^+g^+ state (Table 2). The dynamic nature of this site is emphasized by the relatively high thermal B factors for main chain atoms and the disulfide in the side chain ($C_\alpha = 45$; $S_\gamma = 78$; $S_\delta = 94$). The B factors for the

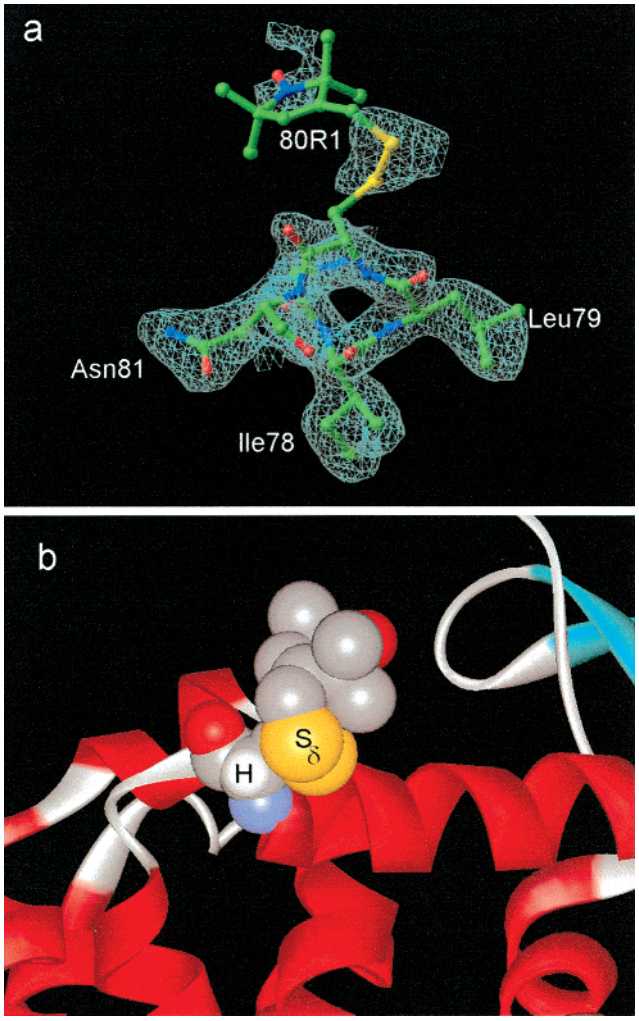

FIGURE 4: (a) Electron density of 80R1 (cyan wire frame), calculated as an unweighted $2F_{obs}$-F_{calc} map contoured at 1.3 σ, with phases from the corresponding model in Table 1. For clarity, and to focus attention on the structure of the nitroxide side chain, electron density is shown only for the R1 side chain and nearby residues in the same helix. The view shown is down the axis of the helix, viewed from the C-terminus. (b) Space-filling model of the R1 side chain showing the position of the disulfide relative to the backbone and the proximity of the Sδ to the hydrogen atom (H) on C_α. The values of X_4 and X_5 were selected from a set of values with minimum steric interference involving the nitroxide ring and are not unique. In this and following figures, the electron density maps were generated in Ribbons (*33*) and the molecular models, including added hydrogen atoms, were generated in WebLab ViewerPro (MSI, Inc., San Diego, CA).

sulfur atoms reflect RMS displacements of approximately ±1 Å. The higher B factor for S_δ as compared to S_γ presumably reflects torsional oscillations about X_2.

In the g^+g^+ conformation of R1, S_δ of the disulfide lies in proximity to the position of the H atom on C_α of the same residue (separation ≈ 3.3 Å, Figure 4b). This is close to the sum of the van der Waals radii (3.1 Å), suggesting the possibility of the S_δ··HC_α attractive interaction identified by Scheraga and coworkers (*21*) (see Discussion).

Structure of 119 R1. The EPR spectrum of 119R1 in solution (Figure 3b, light trace) has two well-resolved components, one corresponding to a nitroxide population of high mobility (labeled α) and the other of lower mobility (labeled β). Crystallization slightly suppresses the mobility of each component and slightly changes the relative popula-

Table 2: Summary of Side Chain Dihedral Angles[a] and Rotamer Designation[b]

mutant	X_1	X_2	X_3	X_4
80R1	286 (g^+)	294 (g^+)		
119R1-conformation 1	310 (g^+)	310 (g^+)		
119R1-conformation 2	175 (t)	54 (g^-)		
65R1	153	89	53	
75R1	287 (g^+)	173 (t)	91	95

[a] The dihedral angle (X) for the central bond in a linear group of four atoms is defined so that 0° corresponds to the position where atoms 1 and 4 are eclipsed, and counterclockwise rotations are positive. For X_1, the main chain nitrogen is taken as atom 1. [b] The criteria for the rotamer designations g^+, g^-, and t are ±20° about 300° (g^+), 60° (g^-), and 180° (t), respectively.

tions of the components. However, the general features of the motion are remarkably well-preserved in the crystal, indicating that the conformation and interactions of the side chain are preserved as well.

A striking feature of the 119R1 electron density map is the resolution of two distinct orientations of the disulfide group (Figure 5a), corresponding to two conformations of the side chain. Conformation 1 (Figure 5, panels a and b) is a g^+g^+ conformation similar to that observed in 80R1 (X_1 = 310, X_2 = 310). In this case, the $C_\alpha H \cdot\cdot S_\delta$ distance estimated from modeling is 3.0 Å. Conformation 2 is a tg^- state (X_1 = 175, X_2 = 54) wherein the disulfide lies close to the side chain amide group of Gln123 at the i + 4 position (Figure 5, panels a and c). Specifically, the S_γ of the disulfide is 3.6 Å above the plane of the amide group, with the $S_\gamma \cdot\cdot N\epsilon 2 \cdot\cdot C_\delta(=O)$ angle ≈ 30°, where $N\epsilon 2$ and C_δ are in the Gln123 side chain. This geometry, in which S_γ is approximately over $N\epsilon 2$, is achieved by a rotation of the side chain amide group of residue Gln123 relative to the position in the native protein. This constitutes the only example of the four cases reported here in which an R1 interaction caused a significant reorientation or displacement of a native side chain. The significance of this configuration will be discussed below. Although not visible in Figure 5, S_δ again lies close to the hydrogen atom on its own $C_\alpha H$, with a $C_\alpha H \cdots S_\delta$ distance of 3.0 Å.

Structure of 65R1. In solution, the EPR spectrum of 65R1 (Figure 3c, thin trace) is similar to those of other helix surface sites (*5*, *9*). However, in the crystal, the spectrum corresponds to a highly immobilized state that could only arise from new interactions of R1 in the crystal. Indeed, the crystal structure shows 65R1 to be at a contact site in the crystal lattice, as discussed below.

The electron density map of 65R1 reveals a strained conformation unlike that for R1 at any of the other sites (Figure 6a). The X_1 of 153° does not fall within the range of the usual states of minimum energy (see Table 2) and this results in steric interference between S_γ and the backbone C(=O) atom of the same residue. The X_2 of 89° lies at the edge of the observed range for a relaxed structure. Because some electron density is resolved for the nitroxide ring, it is possible to estimate X_3, the disulfide dihedral angle. For 65R1, X_3 = 53°, a distortion of more than 30° from the minimum energy configuration of 85°.

A number of favorable intra- and intermolecular contact interactions appear to at least partially offset the apparent strain in 65R1. For example, the i + 4 glutamine residue (Gln69) contacts the disulfide, as in conformation 2 of 119R1, but the Gln69 side chain has not reoriented from the native conformation. The closest contact is between NE2 of Gln69 and the S_γ of 65R1 at a distance of 3.3 Å and a $S_\gamma \cdot\cdot NE2 \cdot\cdot C(=O)$ angle of approximately 40° (Figure 6, panels b and c).

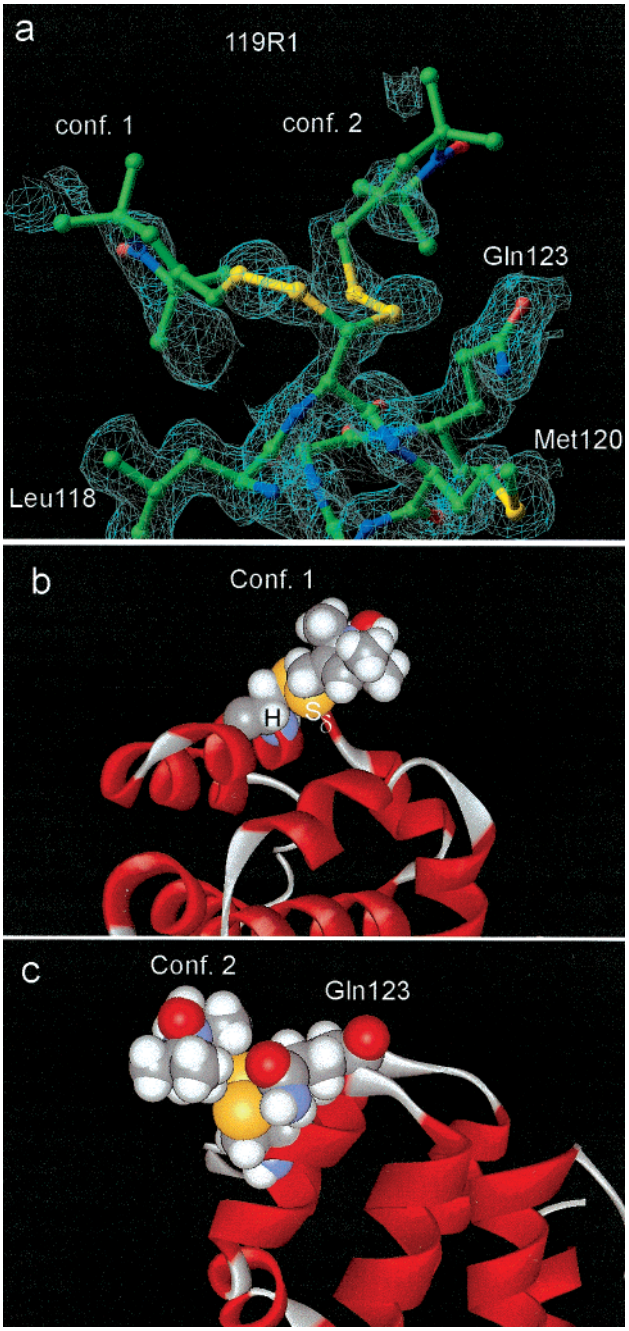

FIGURE 5: (a) Electron density of 119R1 (cyan wire frame), calculated as an unweighted $2F_{obs}$-F_{calc} map contoured at 1.3 σ, with phases from the corresponding model in Table 1. For clarity, and to focus attention on the structure of the nitroxide side chain, electron density is shown only for the R1 side chain and nearby residues in the same helix. The view is along the helical axis, viewed from the N-terminus. Two conformations of the side chain, differing in both X_1 and X_2, are clearly resolved from the discrete electron densities corresponding to the disulfide groups. (b) Space-filling model of conformation 1, emphasizing the similarity to 80R1. (c) Space-filling model of conformation 2, showing the contact of the disulfide with Gln123 in the i + 4 position. Values of X_4 and X_5 were selected from a set of values with minimum steric clash involving the nitroxide ring and are not unique.

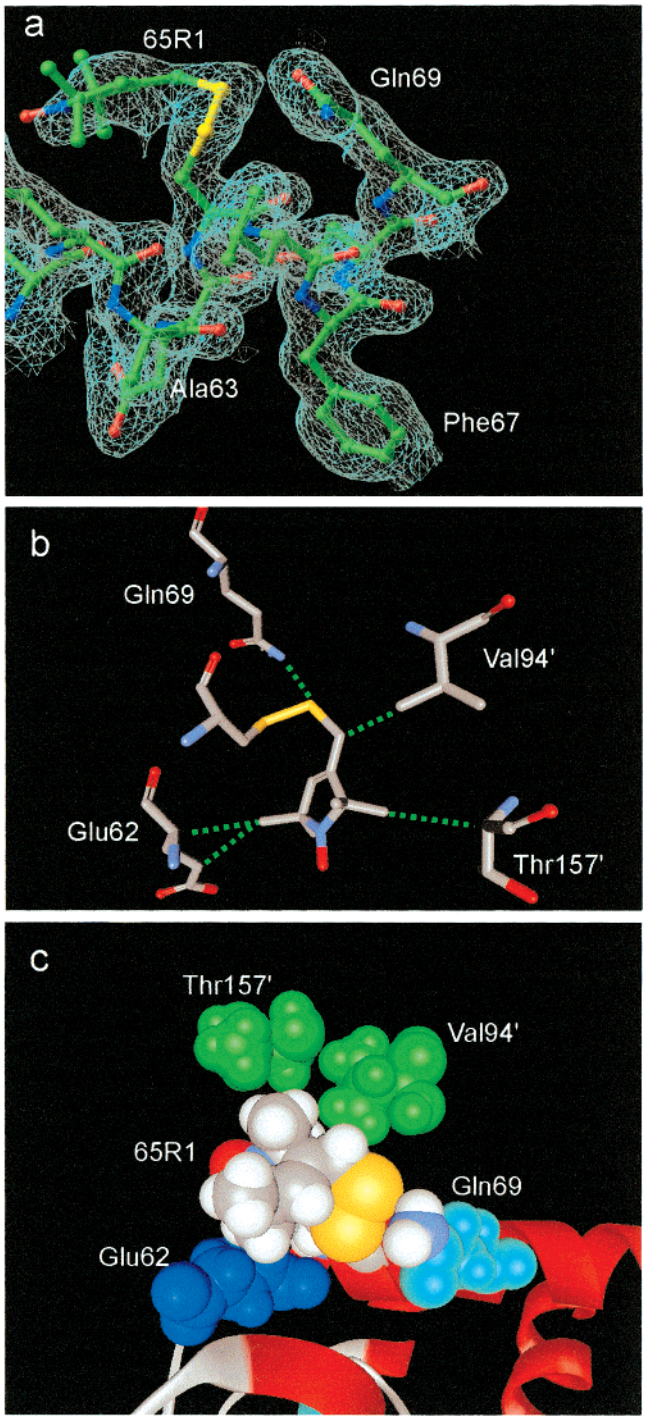

FIGURE 6: (a) Electron density of 65R1 (cyan wire frame), calculated as an unweighted $2F_{obs}$-F_{calc} map contoured at 1.3 σ, with phases from the corresponding model in Table 1. For clarity, and to focus attention on the structure of the nitroxide side chain, electron density is shown only for the R1 side chain and nearby residues in the same helix. The view is perpendicular to the helical axis. (b) Stick model of 65R1 and proximal residues. Primed (′) residues are from a symmetry related molecule at this crystal contact site. Dotted lines indicate potential contact interactions. (c) Space-filling model showing the 65R1 environment in T4L. Hydrogen atoms were added and the nitroxide ring was modeled in WebLab ViewerPro (MSI, Inc., San Diego, CA) to illustrate the putative contact interactions that immobilize the 65R1 side chain.

Although the α-methyl groups of the nitroxide ring are not resolved in the electron density, modeling indicates that one -CH_3 group of the nitroxide ring could make van der Waals contact with the $C_\alpha H$ and $C_\gamma H_2$ groups of the Glu62 side chain, as shown in Figure 6, panels b and c. However, these interactions alone are insufficient to immobilize the nitroxide in solution (Figure 3c, light trace). Apparently, the immobility in the crystal arises from the intermolecular interactions with a symmetry related molecule in the lattice, as illustrated in Figure 6, panels b and c. Likely interactions are between C_ϵ in R1 and the $C_\gamma 2$ of Val94 (3.4 Å) and a -CH_3 group of the nitroxide ring with C_α and C_β carbons of Thr157. The B factors for 65R1 65 ($C_\alpha = 25$; $S_\gamma = 41$; $S_\delta = 72$) reflect a more highly ordered side chain as compared to 80R1, consistent with the contact interactions.

Structure of 75R1. Residue 75R1 lies at a tertiary contact interface between two helices, and the EPR spectrum of 75R1 in solution corresponds to a state with a highly constrained motion of the nitroxide (Figure 3d, light trace). The spectrum of 75R1 in the crystal is extremely broad (Figure 3e). Such great spectral breadth can only arise from magnetic spin−spin interactions. This conclusion is clearly supported by the crystal structure, which shows that two 75R1 side chains lie along a 2-fold symmetry axis at a crystal contact (see below).

Figure 7a shows the electron density map for R1 at site 75, where electron density is resolved for the entire side chain. Unlike the case for 65R1, the immobilized side chain of 75R1 is confined to a single conformation whose high degree of order is reflected in the B factors ($C_\alpha = 23$; $S_\gamma = 25$; $S_\delta = 25$) The interactions that immobilize the 75R1 side chain are of both intra- and intermolecular origin, as for 65R1.

The intramolecular interactions that cause this remarkably ordered structure arise partially from contacts between an α-methyl group of the nitroxide ring and $C_{\delta 1}$ of Ile100, C_α and C_β of Ala97 and C_β of Ala93 (Figure 7b), where the interatomic C−C distances are ≤4.0 Å. Of most interest is an unconventional C−H··O hydrogen bond formed between the hydrogen atom of the sp2-hybridized carbon at the 4 position of the nitroxide ring and the oxygen of Tyr88 (Figure 7b). In this interaction, the overall C···O distance is 3.3 Å. After modeling, the ring H atom, the H- -O distance is 2.2 Å, the C−H··O angle is 158°, and the C−O··H angle is 166°. On the basis of a comparison with the wild-type structure, Tyr88 does not undergo a conformational change to accommodate this interaction.

Two intermolecular contacts are made with side chains from a symmetry-related molecule. First, the N−O of 75R1 approaches Phe4 in the plane of the ring at the position of the para carbon atom. The overall C···O distance is 3.1 Å. After modeling the para-H atom on the benzene ring, the H··O distance is 2.1 Å, the C−H−O angle is 173°, and the N−O−H angle is 125°. Second, a methyl group of 75R1 contacts the methyl group of a symmetry-related 75R1. Because of the proximity of two nitroxides, the magnetic dipolar interaction is strong, consistent with the extreme breadth of the EPR spectrum of 75R1 in the crystal but not in solution.

DISCUSSION

General Features of the R1 Side Chain. An earlier study of 65R1, 80R1, and 75R1 in T4L found that these mutants had essentially wild-type enzymatic activity and produced no (for 65R1) or minor (≈ −1 kCal/mol for 75R1 and 80R1) decreases in the free energy of unfolding (*9*). From these

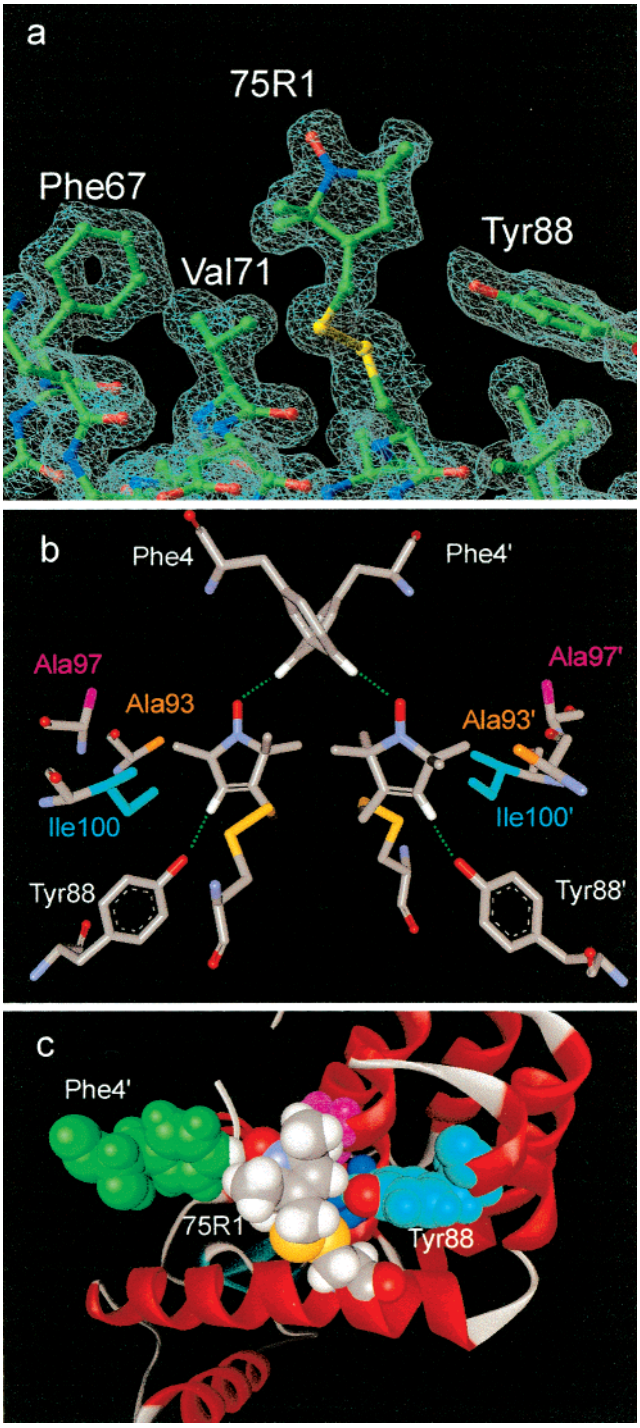

FIGURE 7: (a) Electron density of 75R1 (cyan wire frame), calculated as an unweighted $2F_{obs}-F_{calc}$ map contoured at 1.3 σ, with phases from the corresponding model in Table 1. For clarity, and to focus attention on the structure of the nitroxide side chain, electron density is shown only for the R1 side chain and nearby residues in the same helix. The view is perpendicular to the helical axis. (b) Stick model of 75R1 and proximal residues, both intra- and intermolecular, at this crystal contact site. Primed (′) residues are from a symmetry related molecule. The view is perpendicular to a vertical 2-fold symmetry axis at the center of the figure. Dotted lines indicate probable interactions, and the indicated distances are for H- -O. (c) A space-filling model of 75R1 showing its environment in T4L and the intra- and intermolecular contacts with Tyr88 and Phe4′, respectively. Residues Ile100 (blue) and Ala97 (violet) can be seen behind 75R1. Hydrogen atoms were added in WebLab ViewerPro (MSI, Inc., San Diego, CA).

results and others, it was concluded that the R1 side chain, when substituted on solvent-exposed helical surface sites, apparently causes little structural perturbation at the level of the backbone fold. This is particularly significant for cases such as 75R1 that involve tertiary interactions with adjacent helices. Each of the spin labeled T4L structures reported here is essentially identical to the wild type at the level of the backbone fold, a result that offers direct structural evidence for the correctness of this conclusion for the mutants studied here.

For each structure investigated, electron density is resolved for the disulfide group of the R1 side chain, indicating that the disulfide group is localized in space. This in turn implies constrained values of the dihedral angles X_1 and X_2. Furthermore, rotation about X_3, the disulfide dihedral angle, has an activation energy of ≈7 kCal/mole (*22*) and is thus slow on the EPR time scale. Together, these data suggest that the mobility of the R1 nitroxide may have its most important contributions from rotations about the two terminal bonds (X_4 and X_5, Figure 1), a result anticipated from analysis of R1 EPR spectra in T4L (*9*). Indeed, the EPR spectra for solvent-exposed helix surface sites can be accurately simulated with this assumption (Columbus, Kálái, Hideg, and Hubbell, unpublished observation). This being the case, immobilized states of R1 must arise from interaction of the nitroxide ring with the protein. As shown above, such interactions are in fact observed for the immobilized states of 65R1 and 75R1.

Table 2 summarizes values of the dihedral angles for the R1 side chain at the four sites investigated. Excluding the crystal contact site 65R1, which is in a strained configuration, there are only two conformations about X_1 observed, corresponding to g^+ and *t*. This is similar to the situation for cysteine itself in α-helical structures, where the g^+ and *t* states are favored over g^- due to steric repulsions of the S_γ with main chain atoms in the latter state (*23*). The values assumed for X_2 are dependent on the specific R1 interactions and will be discussed separately for each side chain below.

Conformation of R1 at Helix Surface Sites Not Involved in Crystal Contacts. Positions 80R1 and 119R1 are examples of helix surface sites that are not at crystal contacts, for which there are no obvious tertiary interactions and that should be in a relaxed configuration. The similarity of the EPR spectra for these mutants in the crystal and in solution confirms that the motion at these sites is not strongly affected by the crystal environment. Thus, we assume that the crystal structures represent the side chain conformation in solution.

Residues 80R1 and 119R1(conformation 1) both reside in the g^+g^+ configuration about X_1, X_2 (Table 2). Why is this configuration stable when many other values of X_2 are allowed on steric grounds? In an early study of cystine conformation in proteins, Van Wart and Scheraga (*21*) concluded that a weak attractive interaction between S_δ of the disulfide and the $C_\alpha H$ hydrogen atom of the same residue, termed a "1-4 interaction", could explain a population of X_2 values as large as 330°. As shown in Figures 4b and 5b, the g^+g^+ configuration places S_δ close to the H atom of its own $C_\alpha H$, and a 1-4 interaction may stabilize the rotamer. This model could also explain the fact that removing the S_δ from the R1 side chain (to produce a thioether-linked side chain) results in an increase in nitroxide mobility, although the number of bonds between the nitroxide and the backbone is fewer (*9*). The nature of the $C_\alpha H\cdots S$ interaction is unknown. However, the $C_\alpha H$ hydrogen is mildly acidic and capable of

forming hydrogen bonds (*24*), and sulfur may act as a hydrogen bond acceptor (*25*). It is thus possible that the 1-4 interaction is an example of weak hydrogen bond to sulfur.

In the tg^- configuration 2 of 119R1, the $C_\alpha H$ hydrogen is also in intimate contact with the S_δ sulfur, and the 1-4 interaction may contribute to the stability of this configuration as well. However, the feature that distinguishes conformation 2 from conformation 1 in 119R1 is the interaction of the disulfide with Gln123 in the i + 4 position in the former (see Figure 5c). The geometry of this interaction (see Results) is well within the criteria recently outlined by Pal and Chakrabarti (*23*) for an apparent S···N interaction that is distinct from hydrogen bonding. Moreover, it was recently shown that the mutation Gln123Ala produces a dramatic decrease in the nitroxide mobility at 119R1(*5*). This lends support to the existence of the proposed Gln123−disulfide interaction, because it seems unlikely that a single Ala residue introduced at 123 could immobilize the nitroxide. Rather, the result suggests that the g^+g^+ state is the more stable configuration in the absence of interactions, and that tg^- relaxes to the g^+g^+ state in the Gln123Ala mutant.

The two-state nature of the disulfide in 119R1 provides a structural basis for the origin of two components in the EPR spectrum. If the environment of the nitroxide ring is sufficiently different in the two rotamers, two components would be observed in the EPR spectrum. This model is supported by the fact that the two states are approximately equally populated in both the EPR spectrum and the electron density map. That the two spectral states arise from two conformations of the side chain is not a trivial conclusion, because it is also possible that they arise from two states of the protein in equilibrium. Indeed, this situation was previously observed in spin labeled hemoglobin (*26*).

From the structural data, it is not possible to deduce which of the 119R1 conformations corresponds to the more immobilized state, or what interaction(s) of the ring lead(s) to immobilization. However, the effect of the Gln123Ala mutation mentioned above suggests that conformation 2, stabilized by the Gln123 interaction, is the more mobile state. The crystallographic data show that the nitroxide ring is disordered in both conformations, suggesting that whatever the immobilizing interactions are in conformation 1, they are nonspecific.

*Conformation and Interactions of R1 Residues at Crystal Contacts***.** Residues 65R1 and 75R1 reside at crystal contact sites. Thus, the conformations of the side chain in the crystal may not correspond to those in solution. Nevertheless, these sites offer a first look at some of the important interactions that result in immobilization of the nitroxide ring and may be considered models for the R1 side chain at buried sites.

In 65R1, the R1 chain appears to be highly strained, and its conformation is apparently shaped by the necessity to avoid steric overlap with nearby side chains in the protein. The X_1 and X_2 values of 65R1 are displaced by ≈30° from their minimum energy configurations. The magnitude of the strain energy involved in this distortion is not large enough to destabilize the crystal lattice or result in reorientations of the native side chains in the contact region.

A number of interactions at least partially compensate for the strain in 65R1. As in the case of 119R1, conformation 2, an i + 4 glutamine residue makes contact with the disulfide (Figure 6, panels b and c) and has an appropriate geometry for a S···N non-hydrogen bonding interaction (*23*). Intra- and intermolecular interactions involving the nitroxide ring, and resulting in its immobilization, are essentially nonspecific and hydrophobic in nature (Figure 6, panels b and c). The fact that electron density is not resolved for the entire ring likely reflects multiple orientations of the nitroxide, consistent with weak, nonspecific interactions. For example, a number of different rotamers about X_5 would avoid steric interference but still make favorable hydrophobic interactions. Given that 65R1 is relatively mobile in solution (Figure 3c), the intramolecular hydrophobic interactions with Glu62 identified in the crystal are by themselves too weak to overcome the strain energy necessary to achieve the 65R1 conformation and the entropic loss of immobilizing the nitroxide ring.

The structure of 75R1 is more informative. In solution, this residue is at a partially solvent-exposed tertiary contact site with an EPR spectrum corresponding to a single, immobilized population. The 75R1 residue is unique among the structures determined in that electron density is clearly resolved for the entire side chain, including the nitroxide ring. Thus, 75R1 is not only immobilized but is also highly ordered. In agreement with its original classification as a tertiary contact site, the crystal structure of 75R1 reveals several intramolecular tertiary contacts of R1 with residues on neighboring helices. Some of these contacts are hydrophobic, but of most interest is the CH···O hydrogen bond between the phenolic oxygen of Tyr88 and the H atom on the sp^2 hybridized carbon of the nitroxide ring. The C···O distance of 3.3 Å is within the 3.0−4.0 Å range observed for CH···O hydrogen bonds in a wide range of small molecules and proteins, and the nearly linear arrangement of the CH···O atoms is consistent with a bond of this type (*24*, *27*). Modeling indicates that the O··H distance in this interaction is 2.2 Å. Precedent for a sp^2 carbon as a H donor in a CH··O bond is provided by the recent studies of Musha et al. (*28*) on the binding of trimethylthiazole to an engineered cavity in cytochrome *c* peroxidase. Peireddi and Desiraju (*29*) have shown that for unhindered interactions, the length of a CH−O hydrogen bond is linearly related to the pK_a of the hydrogen on the donor. Using their relationship, the 3.3 Å C··O distance observed here predicts a pK_a of ≈22 for the 4-H atom on the nitroxide ring. The CH··O hydrogen bonds are expected to provide stabilization in the range of 1−4 kcal/mole (*25*, *30*).

In addition to the intramolecular interactions, crystal contacts are made with another R1 side chain and Phe4 in a symmetry related molecule in the lattice. The interaction between R1's is a limited hydrophobic contact. In the interaction with Phe4, the electronegative oxygen of the N−O makes an "edge-on" contact with an H atom of the aromatic ring. The C··O distance of 3.1 Å (estimated H··O distance of 2.1 Å), the essentially linear arrangement of the CH··O group, and the partial positive charge on the H atom of the aromatic ring strongly indicate another CH··O hydrogen bond interaction, this time with the nitroxide as the acceptor.

These crystal contact interactions will act to constrain the motion of the 75R1 nitroxide in the crystal. However, this residue is also relatively immobilized in solution (Figure 3d), and it is likely that the intramolecular tertiary contacts mentioned above are sufficient to immobilize 75R1 on the EPR time scale, particularly because the 75R1 side chain and neighboring residues are in relaxed conformations. For

example, by favoring the immobilized state with a modest $\Delta G^\circ = -2$kcal/mole, this state would be populated to 97% and dominate the EPR spectrum. The CH··O hydrogen bond, together with the hydrophobic contacts, could easily contribute this stabilization free energy. The notion that the hydrogen bond contributes to the immobilization of the ring in solution is strongly supported by the observation that mutation of Tyr88 to phenylalanine dramatically increases the mobility of 75R1 in solution as judged by the EPR spectrum (Columbus and Hubbell, unpublished observation).

It is likely that nonconventional hydrogen bonds formed between the nitroxide ring and nearby acceptors and donors in the protein contribute to ring immobilization that is characteristic for R1 at tertiary contact and buried sites. Such interactions would account, at least in part, for the fact that a saturated analogue of R1, with a sp^3 hybridized carbon at the 4 position, typically exhibits much higher mobility at the same site (*5*).

The R1 Side Chain as a "Sensor" of Protein Conformation. For a variety of reasons, side chain R1 has become the spin label of choice in SDSL studies. On one hand, R1 is tolerated surprisingly well at the vast majority of sites at which it has been introduced in many different proteins. On the other hand, its EPR spectra are exquisitely sensitive to features of the local environment and provide a fingerprint for virtually every site. The structures presented here explain these important properties. For example, the R1 side chain has five bonds about which rotations can potentially occur. If all of these rotations were realized, effective averaging of the nitroxide magnetic anisotropies would occur, and the R1 spectra would have little sensitivity to features of the surrounding structure. However, the presence of the disulfide linkage, and its interaction with main chain atoms, effectively locks the C_α-C_β-S_γ-S_δ atom group in position and relegates motional averaging to the two terminal bonds adjacent to the nitroxide ring. This limited freedom for rotations places the EPR spectra of R1 side chains on helical surfaces in the range of maximum sensitivity to detect interactions of the nitroxide ring with nearby structures (at X-band frequencies). In addition, the disulfide-backbone interaction serves to couple backbone fluctuations to nitroxide motion, making it feasible to map backbone dynamics with R1 side chains on exposed surfaces.

Why is R1 so well-tolerated in proteins, even at buried sites? A unique feature of R1 is that weak interactions of the disulfide constrain internal side chain motion about all except the two terminal bonds. However, because the constraints are weak, R1 is able to access a manifold of conformations to minimize steric clashes at buried and tertiary contact sites. Thus, R1 achieves a delicate balance of interaction energy such that it has little internal flexibility on surface sites but has effectively high flexibility in constrained sites. This latter point is nicely illustrated by the 65R1 structure in the crystal, which can be taken as a model for a buried site.

One of the most useful quantities in structure mapping with SDSL is interresidue distance estimated from the strength of the magnetic dipolar interaction between two R1 side chains. In principle, it is possible to measure interspin distances with great accuracy (*31*). However, it is evident from the structures presented here that the conformational equilibria of the R1 side chain, and not the theory, will limit the resolution, severely in some situations. For example, the nitroxides in the two conformations of 119R1 are separated by $\approx$7 Å. In the worst case of two R1's, each with two conformations, aligned so that the displacements are along the interspin vector, the distance could vary by as much as 14 Å. This extreme case is relatively improbable, and other relative orientations of the R1 side chains would result in much less possible variation. In addition, large changes in apparent interspin distance during a conformational change in the protein could in fact arise from conformation changes of the side chain.

Errors of this type, associated with the spatial distribution of the spins, are avoided by selecting sites that have unique conformations. Although more structures are needed to build a reliable database, it appears that R1 on helix surfaces sites, in the absence of nitroxide interactions, has a preferred g^+g^+ conformation about X_1, X_2, and rotations about X_4 and X_5 produce little displacement of the nitroxide (X_3 is fixed on the EPR time scale). These simple cases are generally recognizable as having single component EPR spectra; multiple components likely reflect multiple side chain conformations.

With the information on the R1 side chain and its interactions provided here, it is feasible to engineer sites of high sensitivity for detection of specific conformational changes in a protein. For example, relative motion of two structural elements should be detected by an R1 side chain in one that is constrained by an appropriately oriented hydrogen bond acceptor or donor in the other. Because of the strong directional and distance dependence of the hydrogen bond energy, relative displacements and/or rotations should be detected with great sensitivity through dynamics changes in the nitroxide ring. This approach is a viable means for investigating structure−activity relationships with high sensitivity in membrane proteins of arbitrary molecular weight. Applications have already been realized in the photoreceptor rhodopsin (*32*), and it should be possible to extend these quite generally to other receptors.

ACKNOWLEDGMENT

We thank Dr. David Eisenberg for providing access to the diffraction facilities in the D.O.E. Laboratory of Structural Biology at UCLA, Dr. Brian Matthews and Blaine Mooers for suggesting the crystallization and cryoprotection conditions for T4 lysozyme and helpful discussions, Dr. James Trudell for helpful discussions on the nature of unconventional hydrogen bonds, and Malcom Capel and the staff of beamline X12B and X8C of Brookhaven National Laboratories for their support with data collection. The model coordinates and diffraction data will be deposited at the Protein Data Bank.

REFERENCES

1. Hubbell, W. L., and Altenbach, C. (1994) *Curr. Opin. Struct. Biol. 4*, 566−573.
2. Hubbell, W. L., Mchaourab, H., Altenbach, C., and Lietzow, M. (1996) *Structure 4*, 779−783.
3. Hubbell, W. L., Gross, A., Langen, R., and Lietzow, M. (1998) *Curr. Opin. Struct. Biol.* 8, 649−656.
4. Feix, J. B., and Klug, C. S. (1998) in *Biological Magnetic Resonance, Vol. 14, Spin Labeling: The Next Millenium* (Berliner, L. J., Ed.) pp 251−281, Plenum Press, New York.

5. Mchaourab, H., Kalái, T., Hideg, K., and Hubbell, W. L. (1999) *Biochemistry 38*, 2947−2955.
6. Altenbach, C., Flitsch, S., Khorana, H., and Hubbell, W. (1989) *Biochemistry 28*, 7806−7812.
7. Griffith, O. H., Dehlinger, P. J., and Van, S. P. (1974) *J. Membr. Biol. 15*, 159−192.
8. Gross, A., Columbus, L., Hideg, K., Altenbach, C., and Hubbell, W. L. (1999) *Biochemistry 38*, 10344−10335.
9. Mchaourab, H., Lietzow, M., Hideg, K., and Hubbell, W. L. (1996) *Biochemistry 35*, 7692−7704.
10. Budil, D. E., Lee, S., Saxena, S., and Freed, J. H. (1996) *J. Magn. Reson. 120*, 155−189.
11. Barnes, J., Liang, Z., Mchaourab, H., Freed, J., and Hubbell, W. L. (1999) *Biophys. J.* 76, 3298−3306.
12. Matsumara M., and Matthews, B. W. (1989) *Science 243*, 792−794.
13. Ho, S. N., Hunt, H. D., Horton, R. M., Pullen, J. K., and Pease, L. R. (1989) *Gene 77*, 51−59.
14. Sauer, U. H., Dao-pin, S., and Matthews, B. W. (1992) *J. Biol. Chem. 267*, 2393−2399.
15. Weaver, L. H., and Matthews, B. W. (1987) *J. Mol. Biol. 193*, 189−199.
16. Otwinowski, Z., and Minor, W. (1993) *Data Collection and Processing*, Daresbury, UK.
17. Brunger, A. T. (1992) X-PLOR, Version 3.1, A System for X-ray Crystallography and NMR, Yale University Press, New Haven, CT.
18. Sheldrick, G. M., and Schneider, T. R. (1997) *Methods Enzymol. 277*, 319−343.
19. Jones, T. A., Zou, J. Y., Cowan, S. W., and Kjeldgaard, M. (1991) *Acta Crystallogr. A47*, 110−119.
20. Hubbell, W. L., Froncisz, W., and Hyde, J. S. (1987) *Rev. Sci. Instrum. 58*, 1879−1886.
21. Van Wart, H. E., and Scheraga, H. A. (1977) *Proc. Natl. Acad. Sci. U.S.A. 74*, 13−17.
22. Jiao, D., Barfield, M., Combariza, J. E., and Hruby, V. J. (1992) *J. Am. Chem. Soc. 114*, 3639−3643.
23. Pal, D., and Chakrabarti, P. (1998) *J. Biomol. Struct. Dyn. 15*, 1059−1072.
24. Derewenda, Z. S., Lee, L., and Derewenda, U. (1995) *J. Mol. Biol. 252*, 248−262.
25. Burley, S. K., and Petsko, G. A. (1988) *Adv. Protein Chem. 19*, 125−189.
26. Moffat, J. K. (1971) *J. Mol. Biol.* 55, 135−146.
27. Desiraju, G. R. (1996) *Acc. Chem. Res. 29*, 441−449.
28. Musah, R. A., Jensen, G. M., Rosenfeld, R. J., McRee, D. E., and Goodin, D. B. (1997) *J. Am. Chem. Soc. 119*, 9083−9084.
29. Pedireddi, V. R., and Desiraju, G. R. (1992) *J. Chem. Soc., Chem Commun*. 988−990.
30. Chakrabarti, P., and Chakrabarti, S. (1998) *J. Mol. Biol. 284*, 867−873.
31. Hustedt, E. J., Smirnov, A. I., Laub, C. F., Cobb, C. E., and Beth, A. H. (1997) *Biophys. J.* 74, 1861−1877.
32. Yang, K., Farrens, D., Hubbell, W. L., and Khorana, H. G. (1996) *Biochemistry 35*, 12464−12469.
33. Carson, M. (1977) *Methods Enzymol.* 277, 493−505.

BI000604F